

Anomalously Low Strength of Serpentinite Sheared against Granite and Implications for Creep on the Hayward and Calaveras Faults

D. E. Moore, D. A. Lockner, and D. A. Ponce, U. S. Geological Survey, Menlo Park, CA 94025

Submitted to: Proceedings of the Third Conference on Earthquake Hazards in the Eastern San Francisco Bay Area — Science, Hazard, Engineering and Risk, edited by K. Knudsen and others, California Geological Survey Special Publication, 2010.

ABSTRACT

Serpentinized ophiolitic rocks are juxtaposed against quartzofeldspathic rocks at depth across considerable portions of the Hayward and Calaveras Faults. The marked compositional contrast between these rock types may contribute to fault creep that has been observed along these faults. To investigate this possibility, we are conducting hydrothermal shearing experiments to look for changes in frictional properties resulting from the shear of ultramafic rock juxtaposed against quartzose rock units. In this paper we report the first results in this effort: shear of bare-rock surfaces of serpentinite and granite, and shear of antigorite-serpentinite gouge between forcing blocks of granitic rock. All experiments were conducted at 250°C. Serpentinite sheared against granite at 50 MPa pore-fluid pressure is weaker than either rock type separately, and the weakening is significantly more pronounced at lower shearing rates. In contrast, serpentinite gouge sheared dry between granite blocks is as strong as the bare granite surface. We propose that the weakening is the result of a solution-transfer process involving the dissolution of serpentine minerals at grain-to-grain contacts. Dissolution of serpentine is enhanced by modifications to pore-fluid chemistry caused by interaction of the fluid with the quartz-bearing rocks. The compositional differences between serpentinized ultramafic rocks of the Coast Range Ophiolite and quartzofeldspathic rock units such as those of the Franciscan Complex may provide the mechanism for aseismic slip (creep) in the shallow crust along the Hayward, Calaveras, and other creeping faults in central and northern California.

INTRODUCTION

Soon after fault creep was first recognized (Steinbrugge and Zacher, 1960; Tocher, 1960), a close association of creeping faults with outcrops of serpentinite was noted (e.g., Allen, 1968; Hanna et al., 1972; Irwin and Barnes, 1975). Numerous laboratory investigations on the frictional properties of serpentinite have been undertaken to determine how it might be responsible for the creeping motion. It was found that the serpentine minerals have the potential to slide unstably under certain conditions (velocity-weakening behavior) (Reinen et al., 1991,

1992, 1994; Moore et al., 1997), making it unlikely that they themselves could be the cause of fault creep. However, along creeping faults, serpentinite typically is juxtaposed against crustal rocks rich in quartz and feldspar that have a very different chemistry from ultramafic mantle rock. Might the chemical contrast between serpentinite and felsic rocks play a role in the development of fault creep?

We have initiated a laboratory investigation designed to test if contrasting rock chemistry across or within a fault can influence the frictional properties of the fault. In this paper we present the results of preliminary experiments shearing serpentinite against granitic rock, which demonstrate the existence of a marked weakening effect under water-saturated conditions that is more pronounced at slower shearing rates. We discuss these results in the context of creep along the Hayward and Calaveras Faults.

EXPERIMENTAL PROCEDURES

We report here on our first sliding tests using serpentinite and granitic rock. The serpentinite is the same antigorite-rich serpentinite from New Idria, California, that we have used in previous studies (e.g., Moore et al., 1997; Moore and Lockner, 2007). It contains ~76 modal % antigorite, ~12% magnetite, ~8% calcite, ~3% chlorite, and minor amounts of other minerals; the rock description and mineral compositions are in Moore et al. (1996). Westerly granite from Rhode Island, which is commonly used in rock-mechanics experiments, served as the representative quartzofeldspathic rock. It is a granodiorite that contains about 40 modal % plagioclase, 25% each quartz and K-feldspar, and 6% biotite, with a variety of accessory and secondary minerals comprising the remainder. Mineral compositions are in Moore et al. (1987).

We ran two sets of strength experiments under hydrothermal conditions (Table 1). One series examined the shear of bare rock surfaces against each other. In the second set of experiments, a layer of antigorite-serpentinite gouge was sheared between forcing blocks of Westerly granite. One additional gouge experiment was run dry, for comparison. To produce the gouge, veins and altered-looking pieces were removed from a crushed sample of the serpentinite. The remainder was then manually ground and passed through a 90- μ m diameter sieve.

All experiments were run at 250°C in a triaxial deformation apparatus, using the furnace assembly shown in Figure 1. The pore-fluid pressure was 50 MPa in the water-saturated experiments. The bare-rock and dry gouge experiments were run at a constant effective normal stress of 100 MPa resolved on the fault surface, and the water-saturated gouge experiments were run at a constant effective confining pressure of 100 MPa (Table 1). The pressure-temperature conditions were chosen with the goal of promoting fluid-assisted processes rather than duplicating fault-zone conditions, but they approximate a depth of burial between 6 and 8 kilometers. The bare-rock samples consisted of a rock cylinder 41 mm long and 19.1 mm in diameter that was cut into two pieces (generally referred to in this paper as ‘driving blocks’) at a 30° angle to the cylinder axis (Fig. 1). The upper driving block contained a throughgoing, 2.4-mm diameter borehole to ensure that the pore fluids used in the water-saturated experiments reached the sawcut surface. Sawcut surfaces were hand lapped with 120-grit SiC to provide a

uniform surface roughness. A 0.13-mm thick greased teflon shim was placed on the end of the piston to provide a low-friction surface to accommodate lateral slip of the lower sample assembly during deformation. The antigorite gouge, where used, was applied as a 1-mm thick layer on the sawcut surface of a Westerly granite driving block. For the water-saturated gouge experiments, a small quantity of 5–10 μm diameter quartz gouge was sprinkled onto the serpentinite gouge layer before the second granite piece was placed on top of it. This was done in an attempt to promote reaction at quartz-serpentine contacts within the gouge. The amount of quartz used was not measured, but it probably comprised <1–2 wt% of the gouge layer.

The sample was placed in a copper jacket between titanium carbide end plugs and alumina insulators. The space between the jacketed assembly and the furnace was loosely packed with boron nitride, a good thermal and poor electrical conductor. Once in the pressure vessel, confining pressure (argon gas) was first increased to 70–80 MPa, while the pore-pressure lines were being evacuated. The evacuation process for water-saturated experiments lasted about 20 minutes; the 50 MPa fluid pressure was then applied, and confining pressure was raised to 150 MPa as the sample was heated. For the one dry experiment, the jacketed sample was dried overnight in a vacuum oven at 120°C (approximately 22 hours). The pore-pressure lines were continuously evacuated during the set-up process and the first few hours of the test (to ~0.1 mm axial displacement).

Temperature was monitored at the top of the sample by a thermocouple inserted along the pore-pressure inlet. Confining pressure was held constant in the wet gouge experiments; constant normal stress was maintained during the bare-rock and dry gouge experiments by means of computer-controlled adjustments to confining pressure. The axial displacement rate was either 0.1 or 0.01 $\mu\text{m/s}$, corresponding to displacement rates along the sawcut surface of ~0.115 or ~0.0115 $\mu\text{m/s}$, respectively. Corrections to the shear strength were made for seal friction, copper jacket strength, and reduction in sliding surface contact area during shearing, as described by Moore and Lockner (2008).

Following the experiments, a thin section was prepared from the dry-gouge sample, and the other samples were removed from their jackets for examination of their textures and mineralogy. Oriented fragments of gouge from the three wet-gouge experiments were examined with a scanning electron microscope (SEM), and the remainder of each gouge layer was disaggregated for bulk X-ray diffraction (XRD) analysis. Entire sawcut surfaces of the bare-rock samples were examined with the backscattered-electron SEM imaging capabilities of an electron microprobe, whose sample chamber was large enough to hold the driving blocks.

RESULTS

Stress-Displacement Measurements

Results of the three bare-rock experiments, with 50 MPa pore pressure, are plotted in Figure 2. These experiments were run at an axial shortening rate of 0.01 $\mu\text{m/s}$, equivalent to a shearing rate of 364 mm per year along a fault. The experiments lasted 2 to 3 days, terminating when the copper jackets failed. Granite sheared against granite is strong; the coefficient of

friction, μ — which is the shear stress divided by the effective normal stress — had reached 0.74 and the sample was still strain hardening when the jacket failed. (Note that because Cu-jacket strength was subtracted from the shear stress after an experiment, all of the strength plots are shifted to the right of the origin.) Antigorite serpentinite is somewhat weaker than granite; μ leveled off at 0.48. When the serpentinite was sheared against granite, the strength initially increased to a peak value at 0.5 mm displacement that was the same as the strength of the all-serpentinite experiment. From that point on, strength decreased continuously, at a relatively rapid rate to ~1 mm axial displacement and more slowly thereafter.

The water-saturated, serpentinite + quartz gouge experiments (Fig. 3) tested time dependence in different ways. The two experiments run at 0.1 $\mu\text{m/s}$ axial displacement rate differed in that one sample sat at the temperature-pressure conditions of the experiment for 2 days before shearing commenced. The 2-day hold made the duration of the experiment close to that of the experiment run at 0.01 $\mu\text{m/s}$. The strength of the antigorite gouge at 0.1 $\mu\text{m/s}$ axial velocity is comparable to that of the bare-rock serpentinite-serpentinite experiment (Fig. 2). Letting the sample sit at elevated temperature and pressure for two days had no effect on measured strength; the two trends are essentially identical following the attainment of peak strength. The 0.1 $\mu\text{m/s}$ experiment run without a hold had an unusually large displacement before reaching peak strength. This probably reflects some slight misalignment of the driving blocks that occurred when the sample was placed in the copper jacket. The two blocks gradually shifted into their proper positions as the sample assembly shortened. The sample tested at 0.01 $\mu\text{m/s}$ reached a peak strength similar to that of the two runs at the faster sliding rate. Strength then decreased throughout the rest of the experiment, with a very pronounced initial drop. The final measured value of μ was 0.35; the difference in strength accompanying an order of magnitude change in shearing rate was $\Delta\mu \geq 0.16$, representing a weakening of more than 30%.

The dry antigorite-serpentinite gouge experiment (Fig. 4) was run at 100 MPa effective normal stress overall. However, the pump that adjusts confining pressure to maintain a constant normal stress stopped working the first night. As a result, confining pressure did not change between about 0.35 and 0.70 mm axial displacement, leading to a gradual increase in effective normal stress to a maximum of 115 MPa. The jump in μ at 0.7 mm axial displacement corresponds to the time that the problem was corrected and effective normal stress returned to 100 MPa. The dry antigorite-serpentinite gouge is ~50% stronger than the water-saturated serpentinite-serpentinite sample (Fig. 2) run at the same sliding rate and is as strong as the granite-granite sample.

Petrography

The serpentinite side of the bare-rock serpentinite-granite sample exhibits well developed slickensides (Fig. 5a, b). A number of tiny pores are visible in close-up views (Fig. 5b); they appear to be dissolution features. Such pores were not seen in previous petrographic studies of the antigorite serpentinite (Moore et al., 1997; Moore and Lockner, 2007). Much of the opposing granite surface is rough, with few features to indicate the direction of shear (Fig. 5c). The slickensides that appear on the granite side typically are developed on coatings of

serpentinite smeared onto the sawcut (Fig. 5d), consistent with the concentration of shear in the weaker serpentinite (Fig. 2).

In typical friction tests on serpentinite gouge, including those from this study, and on most other gouges rich in layer-structure minerals (e.g., Moore and Lockner, 2004, 2007), shearing becomes localized along boundary (B) shears developed within the gouge layer close to the sawcut surfaces and Riedel (R) shears that cross the gouge (Fig. 6a). The gouge away from the shears is relatively undeformed. The gouge layer shown in Figure 6a is the one that was sheared dry. For the three water-saturated, quartz-bearing gouge layers, shear was concentrated in the quartz-free areas such that the sides containing the quartz lack boundary shears (Fig. 6b). The R shears in these samples terminate before they reach the quartz-bearing side. As with the bare-rock serpentinite-granite experiment (Fig. 5), the shear was localized in the weaker serpentinite, avoiding the quartz for which $\mu > 0.7$ at these conditions (Chester and Higgs, 1992). The shear planes developed in these samples, whose surfaces were examined with the SEM, typically show well-developed slickensides (Fig. 6c).

There were few indications of crystal growth during the experiments. The best evidence was for the crystallization of trace amounts of serpentine away from the shears. Small white arrows in Figure 6b point to three small grains of serpentine with euhedral crystal faces (portions of hexagonal platelets). Such textures are not seen in the ground-up starting material. The hexagonal shapes are suggestive of the serpentine variety lizardite (Deer et al., 1962; Mumpton and Thompson, 1975). The bulk XRD analyses of the gouge samples did not reveal the presence of any minerals other than those present in the starting material, although a mineral constituting less than a few percent of the sample would not be detected by this method. In almost all cases, the shear surfaces were composed of the minerals in the starting material. A few tabular crystals of calcium sulfate found on the granite side of the serpentine-granite bare-rock sample appear to be quench products because they grew over and across slickensides. Trace amounts of brucite, $\text{Mg}(\text{OH})_2$, were identified on an R shear from the antigorite gouge experiment run at $0.01 \mu\text{m/s}$ (Fig. 3). Brucite was not identified previously in the antigorite-rich gouge, but brucite is a constituent of the antigorite serpentinite at New Idria (Mumpton and Thompson, 1966, 1975) and thus could be present in minor amounts in the starting material.

DISCUSSION OF RESULTS: WEAKENING AS A SOLUTION-TRANSFER PROCESS

The frictional strength of bare Westerly granite blocks sheared against each other (Fig. 2) is consistent with the strength of Westerly gouge at 250°C under hydrothermal conditions reported by Blanpied et al. (1995). The experimental results for the antigorite serpentinite illustrate two weakening effects. One is the difference between dry and water-saturated serpentinite strength. The dry serpentinite gouge (Fig. 4) is as strong as granite; similar dry antigorite strengths ($\mu \sim 0.8$) were found at room temperature (Morrow et al., 2000) and at 300°C (Moore and Lockner, 2007). Adding water to the serpentinite lowered its strength to $\mu \sim 0.5$, which is consistent with our previous work on water-saturated antigorite serpentinite at elevated temperatures (Moore et al., 1997; Moore and Lockner, 2007). The sheet silicates as a group show marked differences between dry and water-saturated frictional strength, whose origins are discussed by Moore and Lockner (2004). Briefly, the dry frictional strength is directly correlated

with the strength of the (001) or interlayer bond. For sheet silicates with weak (001) bonds, shear occurs by breaking those bonds to form new cleavage surfaces. Dry serpentine is strong because its interlayer bond is sufficiently strong that other frictional processes are favored. Water-saturated strength is lubricated by the stabilization of structured water films between the plate surfaces. The localization of slip to narrow zones in which the platy minerals are oriented subparallel to the shear planes allows shear to be concentrated in the relatively weak water films. The shear strength of the water films is correlated with the strength of the (001) bond, and antigorite is one of the stronger phyllosilicate minerals under water-saturated conditions.

The focus of this study is the second weakening effect that accompanied the addition of granitic rock to the ultramafic-rock system — but only in the presence of water. The wet gouge experiments (Fig. 3) emphasize the very strong positive rate dependence of the weakening (decreased shear rate results in decreased strength). In comparison, an order of magnitude decrease in shearing rate of antigorite gouge housed between blocks of ultramafic rock lowered μ by at most 0.03 (Moore et al., 1997; Moore and Lockner, 2007), and under some conditions strength increased rather than decreased with decreasing velocity. The change in strength due to a change in shear rate shown in Figure 3 is thus at least 5 times larger than previously found for antigorite.

The operation of a fluid-activated, strongly rate-dependent weakening process in the serpentinite is consistent with the solution-transfer creep that has been documented in experiments on quartz (Chester and Higgs, 1992) and granite (Blanpied et al., 1995) at elevated temperatures, and on an analogue system consisting of halite and kaolinite sheared in the presence of brine (Bos and Spiers, 2001). The process involves dissolution at stressed grain contacts, diffusion of the dissolved material away from the stressed site, and recrystallization in a lower-stress region. Both cataclastic (i.e., grain sliding, rolling, and crushing) and solution-transfer processes are operative in rocks throughout the upper crust. At lower temperatures and faster slip rates, cataclastic processes dominate, whereas the pressure-solution process becomes more effective as temperatures increase and shearing rates are reduced. The base of the seismogenic zone, occurring at $\sim 350^\circ\text{C}$ in quartz-bearing crustal rocks, is at the depth where the stress-induced dissolution-precipitation reaction comes to dominance over the cataclastic mechanisms in faults.

Fluid chemistry, particularly pH, affects the solubility of quartz, which in turn will influence solution-transfer processes in felsic rocks. In a similar fashion, we suggest that modifications to the pore-fluid chemistry caused by interaction with minerals in the granite increases the solubility of serpentine and thereby enhances solution-transfer processes during the serpentinite-granite experiments. Changes in pH of the pore fluid may also be important here. Dissolution of serpentine (using the ideal serpentine formula) in water produces hydroxide ion:



and groundwaters emanating from springs in serpentinite bodies have relatively high pH in the range 10.8–12 (e.g., Barnes and O’Neil, 1969; Barnes et al., 1972). In contrast, groundwaters associated with granitic rock have a lower pH. Dissolution of quartz combined with ionization of dissolved silica species in basic pore fluids:



would buffer pH at a lower value (≤ 9) (Krauskopf, 1967), which may in turn enhance serpentine dissolution.

Only minor evidence of mineral dissolution and precipitation of serpentine was seen in these samples (e.g., Figs. 5c and 6b); however the focus of the petrographic work was on the search for new minerals on the shear surfaces. Future petrographic examinations will place greater emphasis on the gouge away from the shears, to look for evidence of serpentine crystallization (Fig. 6b). The textures of natural serpentinite fault gouge support the idea that pressure solution creep is an important process in serpentinite-bearing faults. For example, Andreani et al. (2005) concluded that elongate chrysotile fibers in serpentinite gouge from the Santa Ynez Fault, California, formed by continuous syntectonic crystallization, the end product of a solution-transfer process accompanying fault slip.

One other notable feature of the experiments involving serpentinite in Figures 2 and 3 is that in all cases strength rose initially to a peak value of $\mu \sim 0.5$, and the pronounced weakening effect at the slow velocities began after that point. Bos and Spiers (2001) observed the same behavior in the kaolinite + halite samples that they tested at different sliding rates. They concluded that cataclastic processes were dominant during initial shearing; peak strength corresponded to the development of a throughgoing foliation, after which pressure-solution creep prevailed. Peak strength in the serpentinite gouge samples coincides with the appearance of the boundary and Riedel shears (e.g., Moore and Lockner, 2004). Until then, processes such as grain-size reduction and rotation of grains are necessary to form the shears. In the same way, peak strength in the bare-rock samples may correspond to the generation of a thin layer of slickensided gouge.

This study demonstrates the potential for the shear of serpentinite in the presence of quartzofeldspathic rocks in promoting fault creep. Considerably more work is required, however, to better characterize the extent and parameters of the weakening effect and the processes causing it. Future laboratory studies will include tests on the other serpentine minerals as well as other ultramafic rock types such as dunite. The experimental conditions will be expanded to a wider range of temperatures and sliding velocities. The standard configuration for our frictional sliding experiments (Fig. 1) is not conducive for the collection of the pore fluids that were in contact with the rock/gouge samples. However, we plan to modify the pore-pressure system to a flow-through design for some experiments, which will allow sampling of fluids at the outlet. Also of particular interest are sliding rates that approach the creep rates measured on faults of the San Andreas system. Reaction zones typically form at the contact between ultramafic and non-ultramafic rock types as a result of chemical diffusion across the contact (e.g., Coleman, 1967; Sanford, 1982; Mori et al., 2007). This suggests that, in the long term, new minerals should form in the fault. For example, in the exhumed Zuccale Fault of Elba, Italy, which contains ultramafic and other rock types, Collettini and Holdsworth (2004) found textural evidence for both pressure solution (dissolution seams and fibrous overgrowths) and the growth of phyllosilicates such as talc and chlorite that, together, may have contributed to substantial

weakening and aseismic slip along the fault. Long-duration experiments at very slow shear rates may be favorable for the crystallization of new minerals.

APPLICATION TO THE HAYWARD AND CALAVERAS FAULTS

The geology of the California Coast Ranges is dominated by the Franciscan Complex, Great Valley Sequence and Coast Range Ophiolite (CRO), all of which are components of a former subduction zone. Sediments of the Great Valley Sequence were deposited on top of oceanic lithosphere, now the Coast Range Ophiolite, in a fore-arc basin, and Franciscan sediments were deposited on the subducting oceanic plate. Steepened portions of the Coast Range Fault, the former subduction thrust fault, have been reactivated and now are sections of the present Hayward and Calaveras Faults (e.g., Page, 1982; Ponce et al., 2003; Graymer et al., 2005). Continued tectonism has caused the ophiolite to become increasingly dismembered and discontinuous along these faults (Ponce et al., 2003).

In order to test the applicability of our experimental results to natural fault zones, we compare measured creep rates to geology and infer where serpentinite might occur along the Hayward (H), Central Calaveras (CC), and Southern Calaveras (SC) Fault system. Creep rate data along the Hayward Fault are from Lienkaemper et al. (2001) and data along the Central and Southern Calaveras Fault system are from Wisely et al. (2007). These data show (Fig. 7a) that the average creep rate along the Hayward Fault is about 4-5 mm/yr and that the creep rates along the Central and Southern Calaveras Faults are much higher, averaging about 9-10 mm/yr, although the data are sparse.

A preliminary 3D geologic model (modified from Graymer et al., 2005; Phelps et al., 2008, and Watt et al., 2008), based on geologic and geophysical data, was used to develop a geologic map of the east and west faces of the H-CC-SC Fault system (Figs. 7b, c). Although these maps indicate that mafic and ultramafic rocks are common along much of the fault system, no obvious correlation between creep rate and geology is apparent. One exception is that creep rates appear to be higher in the San Leandro gabbro (km 30-60) compared to those just to the north, which occur in undivided CRO (km 20-30) (Fig. 7b).

In particular, small, discontinuous exposures of serpentinite are exposed along the Hayward Fault from about km 7-14, km 23-30, and km 49-52 (Graymer, 2000), although magnetic data indicate that these bodies are relatively small and shallow. Serpentinite is also exposed intermittently along the western side of the CC-SC Fault from about km 120-138 (Wentworth et al., 1999). Here and further to the south, from about km 138 to 170, aeromagnetic data (hachures, Fig. 7c, d) indicate that serpentinite is present at depth along much of the western side of the fault system (R. Jachens, oral commun., 2009).

Undivided CRO, which includes serpentinite, is exposed along the surface at various locations along the H-CC-SC Fault system, including from about km 22-52 (Fig. 7b, c). At depth, CRO may be present from about km 15-105, based on the preliminary 3D geologic model. In the central part of the Hayward Fault, CRO occurs as the San Leandro gabbro from about km 30-60. Here the lithology is primarily gabbro, but may include some ultramafic rocks such as

pyroxenite and serpentinite, based on small exposures at the surface (e.g., Graymer, 2000, written commun., 2003). CRO also probably extends in the subsurface southward along the H-CC Fault to south San Jose (Fig. 7b) (near Metcalf Road and the junction of Highways 85 and 101), where an outcrop of gabbro occurs near km 100 (Wentworth et al., 1999). Although the exposure is small and does not produce an aeromagnetic anomaly (Ponce et al., 2005), it occurs along the southern edge of a prominent aeromagnetic high (Fig. 7d) probably related to CRO associated with Great Valley basement (Jachens et al., 1995). The westward extent of the Great Valley magnetic anomaly appears to be disrupted and possibly terminated by the Hayward Fault (Jachens et al., 1995); the southern extent of the magnetic anomaly along the fault system terminates at about km 100 (Fig. 7d, e).

Based on these results, serpentinite and undivided CRO probably occur along much of the H-CC-SC Fault system. Our ability to delineate these ultramafic and mafic rocks is, in part, related to their physical property contrasts with surrounding rocks. Physical property measurements on CRO rock samples along the fault system indicate that serpentinite has low average density (2480 kg/m^3) and is moderately magnetic (average susceptibility of 2.79×10^{-3} cgs), whereas gabbro has relatively high average density (2880 kg/m^3) and is weakly to moderately magnetic (average susceptibility of 1.17×10^{-3} cgs) (Ponce et al., 2003). Thus, it should be possible to distinguish between these two rock types. However, the degree of serpentinization in ultramafic rocks may be highly variable and the magnetic properties of other CRO rocks such as basalt and keratophyre are also highly variable, producing interfering anomalies that are difficult to differentiate. Although there is yet no obvious relationship between creep rate and geology, combined geologic and geophysical data indicate that the presence of serpentinite is permissive along much, if not all of the Hayward-Central Calaveras-Southern Calaveras Fault system.

CONCLUSIONS

These preliminary experiments demonstrate that the chemical contrast between ultramafic and quartzofeldspathic rock types can lead to dramatic weakening during slow shear at hydrothermal conditions. The strong rate dependence of weakening suggests that solution transfer (pressure-solution creep) may be the dominant process operative in the time span of the experiments. This chemically driven process may promote stable slip in a fault zone at depths that, in normal continental crust, would be in the seismogenic zone. Because of the occurrence of serpentinized ultramafic rocks of the Coast Range Ophiolite along both the Hayward and Calaveras Faults, such processes may be responsible for the creep variation along fault strike documented on those faults. Indeed, if our hypothesis is correct, active faults in any area where oceanic lithosphere, or other mantle rocks, have been accreted onto a continent are candidates for fault creep.

REFERENCES

Allen, C.R., 1968, The tectonic environments of seismically active and inactive areas along the San Andreas fault system, *in* Dickinson, W.R., and Grantz, A., eds., Proceedings of conference on geologic problems of San Andreas fault system: Stanford University Publications in the Geological Sciences, v. 11, p. 70–80.

Andreani, M., Boullier, A.-M., and Gratier, J.-P., 2005, Development of schistosity by dissolution-crystallization in a Californian serpentinite gouge: *Journal of Structural Geology*, v. 27., p. 2256–2267.

Barnes, I., and O’Neil, J.R., 1969, The relationship between fluids in some fresh alpine-type ultramafics and possible modern serpentinization, western United States: *Geological Society of America Bulletin*, v. 80, no. 10, p. 1947–1960.

Barnes, I., Rapp, J.B., and O’Neil, J.R., 1972, Metamorphic assemblages and the direction of flow of metamorphic fluids in four instances of serpentinization: *Contributions to Mineralogy and Petrology*, v. 35, p. 263–276.

Blakely, R.J., 1995, *Potential theory in gravity and magnetic applications*: Cambridge University Press, 441 p.

Blanpied, M.L., Lockner, D.A., and Byerlee, J.D., 1995, Frictional slip of granite at hydrothermal conditions: *Journal of Geophysical Research*, v. 100, no. B7, p. 13,045–13,064.

Bos, B., and Spiers, C.J., 2001, Experimental investigation into the microstructural and mechanical evolution of phyllosilicate-bearing fault rock under conditions favoring pressure solution: *Journal of Structural Geology*, v. 23, p. 1187–1202.

Chester, F.M., and Higgs, N.G., 1992, Multimechanism friction constitutive model for ultrafine quartz gouge at hypocentral conditions: *Journal of Geophysical Research*, v. 97, no. B2, p. 1859–1870.

Coleman, R.G., 1967, Low-temperature reaction zones and alpine ultramafic rocks of California, Oregon, and Washington: *U.S. Geological Survey Bulletin* 1247, 49 p.

Collettini, C., and Holdsworth, R.E., 2004, Fault-zone weakening and character of slip along low-angle normal faults: Insights from the Zuccale fault, Elba, Italy: *Journal of the Geological Society*, v. 161, p. 1039–1051.

Deer, W.A., Howie, R.A., and Zussman, J., 1962, *Rock-forming Minerals*, vol. 3, Sheet Silicates: John Wiley, New York, p. 170–190.

Graymer, R.W., 2000, Geologic map and map database of the Oakland metropolitan area, Alameda, Contra Costa, and San Francisco Counties, California: U.S. Geological Survey Miscellaneous Field Studies Map MF-2342, 29 p., scale 1:50,000.

Graymer, R., Ponce, D., Jachens, R., Simpson, R., Phelps, G., and Wentworth, C., 2005, Three dimensional geologic map of the Hayward Fault, northern California: Correlation of rock units with variations in seismicity, creep rate, and fault dip: *Geology*, v. 33, no. 6, p. 521–524.

Graymer, R.W., Bryant, W., McCabe, C.A., Hecker, S., and Prentice, C.S., 2006, Map of Quaternary-active faults in the San Franciscan Bay region: U.S. Geological Survey Scientific Investigations Map 2919, scale 1:275,000.

Hanna, W.F., Brown, R.D., Jr., Ross, D.C., and Griscom, A., 1972, Aeromagnetic reconnaissance and generalized geologic map of the San Andreas fault between San Francisco and San Bernardino, California: U.S. Geological Survey Geophysical Investigations Map GP-815, scale 1:250,000.

Irwin, W.P., and Barnes, I., 1975, Effect of geologic structure and metamorphic fluids on seismic behavior of the San Andreas fault system in central and northern California: *Geology*, v. 3, no. 12, p. 713–716.

Jachens, R.C., Griscom, Andrew, and Roberts, C.W., 1995, Regional extent of Great Valley basement west of the Great Valley, California: Implications for extensive tectonic wedging in the California Coast Ranges: *Journal of Geophysical Research*, v. 100, no. B7, p. 112,769–12,790.

Krauskopf, K.B., 1967, *Introduction to Geochemistry*: McGraw-Hill Book Company, New York, 721 p.

Lienkaemper, J.J., Galehouse, J.S., and Simpson, R.W., 2001, Long-term monitoring of creep rate along the Hayward fault and evidence for a lasting creep response to 1989 Loma Prieta earthquake: *Geophysical Research Letters*, v. 28, p. 2265-2268.

Moore, D.E., and Lockner, D.A., 2004, Crystallographic controls on the frictional behavior of dry and water-saturated sheet structure minerals: *Journal of Geophysical Research*, v. 109, B03401, doi:10.1029/2003JB002582.

Moore, D.E., and Lockner, D.A., 2007, Comparative deformation behavior of minerals in serpentinized ultramafic rock: Application to the slab-mantle interface in subduction zones: *International Geology Review*, v. 49, p. 401–415.

Moore, D.E., and Lockner, D.A., 2008, Talc friction in the temperature range 25°–400°C: Relevance for fault-zone weakening: *Tectonophysics*, v. 449, p. 120–132.

Moore, D.E., Lockner, D.A., Summers, R., Byerlee, J.D., and Ma, S., 1996, Sample characterizations and strength measurements of serpentinite gouges: U.S. Geological Survey Open-File Report 96-702, 88 p.

Moore, D.E., Lockner, D.A., Ma, S., Summers, R., and Byerlee, J.D., 1997, Strengths of serpentinite gouges at elevated temperatures: *Journal of Geophysical Research*, v. 102, p. 14,787–14,801.

Moore, D.E., Lockner, D.A., Tanaka, H., and Iwata, K., 2004, The coefficient of friction of chrysotile gouge at seismogenic depths, *in* Ernst, W.G., ed., *Serpentine and Serpentinites: Mineralogy, Petrology, Geochemistry, Ecology, Geophysics, and Tectonics: Geological Society of America International Book Series*, v. 8, p. 525–538.

Moore, D.E., Morrow, C.A., and Byerlee, J., 1987, Fluid-rock alteration and fracture development in ‘crystalline’ rock types: U.S. Geological Survey Open-File Report 87-279, 53 p.

Mori, Y., Nishiyama, T., and Yanagi, T., 2007, Chemical mass balance in a reaction zone between serpentinite and metapelites in the Nishisonogi metamorphic rocks, Kyushu, Japan: Implications for devolatilization: *Island Arc*, v. 16, p. 28–39.

Morrow, C.A., Moore, D.E., and Lockner, D.A., 2000, The effect of mineral bond strength and adsorbed water on fault gouge frictional strength: *Geophysical Research Letters*, v. 27, no. 6, p. 815–818.

Mumpton, F.A., and Thompson, C.S., 1966, The stability of brucite in the weathering zone of the New Idria serpentinite: *Proceedings 14th National Conference on Clays and Clay Minerals*, p. 249–257.

Mumpton, F.A., and Thompson, C.S., 1975, Mineralogy and origin of the Coalinga asbestos deposit: *Clays and Clay Minerals*, v. 23, p. 131–143.

Page, B.M., 1982, The Calaveras fault zone of California — An active plate boundary element, *in* Hart, E.W., Hirschfeld, S.E., and Schulz, S.S., eds., *Proceedings of the Conference on Earthquake Hazards in the Eastern San Francisco Bay Area*, California Division of Mines and Geology Special Publication 62, p. 175–184.

Phelps, G.A., Graymer, R.W., Jachens, R.C., Ponce, D.A., Simpson, R.W., and Wentworth, C.M., 2008, Three dimensional geologic map of the Hayward Fault, California: U.S. Geological Survey Scientific Investigations Map 3045 [<http://pubs.usgs.gov/sim/3045/>].

Ponce, D.A., Hildenbrand, T.G., and Jachens, R.C., 2003, Gravity and magnetic expression of the San Leandro gabbro with implications for the geometry and evolution of the Hayward Fault zone, northern California: *Bulletin of the Seismological Society of America*, v. 93, no. 1, p. 14–26.

Ponce, D.A., Graymer, R.W., Jachens, R.C., Williams, R.A., Simpson, R.W., Wentworth, C.M., and Roberts, C.W., 2005, Southern extension of the Hayward Fault and its relationship to the Calaveras and Silver Creek Faults, northern California [abs.]: *Geological Society of America, Abstracts with Programs*, v. 37, no. 4, p. 90.

Reinen, L.A., Weeks, J.D., and Tullis, T.E., 1991, The frictional behavior of serpentinite: Implications for aseismic creep on shallow crustal faults: *Geophysical Research Letters*, v. 18, p. 1921–1924.

Reinen, L.A., Tullis, T.E., and Weeks, J.D., 1992, Two-mechanism model for frictional sliding of serpentinite: *Geophysical Research Letters*, v. 19, p. 1535–1538.

Reinen, L.A., Weeks, J.D., and Tullis, T.E., 1994, The frictional behavior of lizardite and antigorite serpentinites: Experiments, constitutive models, and implications for natural faults: *Pure and Applied Geophysics*, v. 143, p. 317–358.

Sanford, R.F., 1982, Growth of ultramafic reaction zones in greenschist to amphibolite facies metamorphism: *American Journal of Science*, v. 282, p. 5543–616.

Steinbrugge, K.V., and Zacher, E.G., 1960, Creep on the San Andreas fault. Fault creep and property damage: *Bulletin of the Seismological Society of America*, v. 50, p. 389–396.

Tocher, D., 1960, Creep on the San Andreas fault. Creep rate and related measurements at Vineyard, California: *Bulletin of the Seismological Society of America*, v. 50, p. 396–404.

Watt, J.T., Ponce, D.A., Graymer, R.W., Simpson, R.W., Jachens, R.C., McCabe, C.A., Phelps, G.A., and Wentworth, C.M., 2008, A three-dimensional geologic model of the Hayward-Calaveras Fault junction: Insights from geophysical data [abs.]: *Seismological Research Letters*, v. 70, no. 2, p. 553.

Wentworth, C.M., Blake, M.C., McLaughlin, R.J., and Graymer, R.W., 1999, Preliminary geologic map of the San Jose 30 x 60-minute quadrangle, California: U.S. Geological Survey Open-File Report 98-795, part 7, scale 1:100,000.

Wisely, B.A., Schmidt, D.A., Weldon, R.J., II, 2007, Appendix P: Compilation of surface creep on California faults and comparisons of WGCEP 2007 deformation model to Pacific North American plate motion, in Working Group on California Earthquake Probabilities, The uniform California earthquake rupture forecast, version 2 (UCERF 2): U.S. Geological Survey Open-File Report 2007-1437 and California Geological Survey Special Report 203. [<http://pubs.usgs.gov/of/2007/1437/p/of2007-1437p.pdf>, last accessed March 27, 2009].

Table 1. Summary of Experiments Conducted.

| Experiments | T (°C) | Pore Pressure (MPa) | Effective Pressure/ Normal Stress (MPa) | Axial Velocity ($\mu\text{m/s}$) | Final Value of μ |
|-------------------------------|-------------------|------------------------------------|--|--|--|
| Bare Rock | | | | | |
| Granite/Granite | 250 | 50 | 100 effective normal stress | 0.01 | 0.74 |
| Serpentinite/Serpentinite | 250 | 50 | 100 effective normal stress | 0.01 | 0.48 |
| Serpentinite/Granite | 250 | 50 | 100 effective normal stress | 0.01 | 0.37 |
| Gouge [Granite Blocks] | | | | | |
| Antigorite + quartz grains | 250 | 50 | 100 effective pressure | 0.10 | 0.51 |
| Antigorite + quartz grains | 250 | 50 | 100 effective pressure | 0.01 | 0.35 |
| Antigorite + quartz grains | 250 | 50 | 100 effective pressure | 0.1 (2-day hold time) | 0.50 |
| Antigorite | 250 | 0 (dry) | 100 effective normal stress | 0.01 | 0.76 |

FIGURE CAPTIONS

Figure 1. Furnace apparatus for friction experiments. The jackets hold samples that are 19.1 mm in diameter. These samples, often referred to as ‘driving blocks’ in this paper, are rock cylinders cut at a 30° angle to produce a simulated fault surface. Some experiments (see Table 1) contained a layer of gouge between the sliding surfaces, while other experiments involved bare surface rock-on-rock sliding.

Figure 2. Bare-rock experiments involving antigorite serpentinite and Westerly granite at 250°C, 0.01 $\mu\text{m/s}$ axial displacement rate, and 100 MPa effective normal stress (50 MPa fluid pressure and 150 MPa normal stress). The strength of the copper jacket is subtracted from the shear stress after an experiment, which shifts all of the plots of μ versus axial displacement.

Figure 3. Gouge experiments at 250°C, 100 MPa effective pressure (50 MPa fluid pressure and 150 MPa confining pressure), at two sliding velocities. Each sample consisted of a layer of antigorite-serpentinite gouge with a sprinkling of quartz grains on one surface, placed between granite blocks. The quartz was added to promote a talc-forming reaction, which did not occur. One sample tested at the faster rate sat for two days at the PT conditions of the experiment prior to shearing.

Figure 4. Frictional strength of antigorite-serpentinite gouge sheared dry between Westerly granite forcing blocks at 250°C, 0.01 $\mu\text{m/s}$, and 100 MPa effective normal stress. The sample was dried overnight at 120°C in a vacuum oven before testing, and pore-pressure lines were evacuated for the first 6 hours of the experiment. A problem arose with the pump that adjusts confining pressure to maintain constant normal stress, causing effective normal stress to exceed 100 MPa between 0.35 and 0.70 mm (to a maximum of 115 MPa). This problem was corrected when it was discovered.

Figure 5. Backscattered-electron images of the shear surfaces of the bare-rock serpentinite-granite experiment (Fig. 2); brightness correlates directly with mean atomic number. The direction of movement of a given surface is indicated by a black arrow. a) The serpentinite surface is extensively slickensided. Bright spots are Fe-oxides, some of which (lower right) are smeared out in the direction of shear. b) Close-up of slickensided serpentinite, that has numerous tiny pores on the surface. c) Typical view of the granite sawcut surface, with only faint indications of shear. The medium-gray areas of the surface are quartz and feldspars, and most of the bright patches are biotite. d) The best developed slickensides on the granodiorite sawcut are on smears of serpentinite.

Figure 6. Antigorite gouge textures. a) Photomicrograph of a portion of the serpentinite gouge layer that was sheared dry (Fig. 4). Offset became localized along boundary (B) and Riedel (R) shears, characterized by a reduction in grain size and preferred alignment of the sheet silicates subparallel to the shear planes. The remainder of the gouge was essentially undeformed. b and c). SEM images of the antigorite + quartz gouge layer from the experiment at 0.01 $\mu\text{m/s}$ axial displacement rate (Fig. 3). Black arrows indicate shear direction. b) Backscattered-electron image of part of the quartz-bearing side of the gouge layer, which did not shear during the experiment. Small white arrows point to the upper- and lowermost of three adjoining platy

grains of serpentine that have euhedral crystal faces suggestive of a hexagonal shape. c) Secondary-electron image of slickensided R shear surface, showing the orientation of platy serpentine subparallel to the shear surface.

Figure 7. Comparison of creep rate and geology along the Hayward and Calaveras Faults. a) Creep rate. Black dots, creep rate data on the Hayward Fault (Lienkaemper et al., 2001); red dots, creep rate data on the Calaveras Fault (from Wisely et al., 2007). b) Preliminary geology on the east and c) west faces of the Hayward and Calaveras Faults (modified from Graymer et al., 2005; Phelps et al., 2008; Watt et al., 2008). d) Aeromagnetic map. e) Plan view map of the Hayward and Calaveras Faults. Red lines, Quaternary faults (from Graymer et al., 2006). **Geology:** CRO, undivided Coast Range Ophiolite; Czs, Cenozoic sediments; f, undivided Franciscan Complex; fn, Franciscan Novato Quarry terrane; fsr, Franciscan mélangé; fyb, Franciscan Yolla Bolly terrane; gb, gabbro; Ku, upper Cretaceous rocks; hachures, serpentinite.

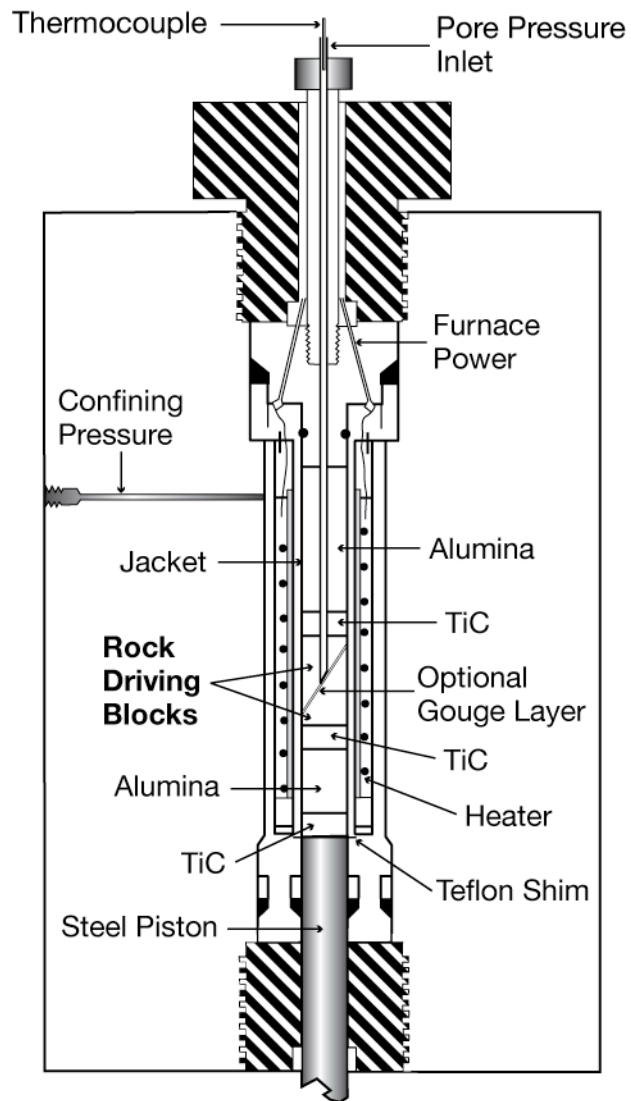


Figure 1

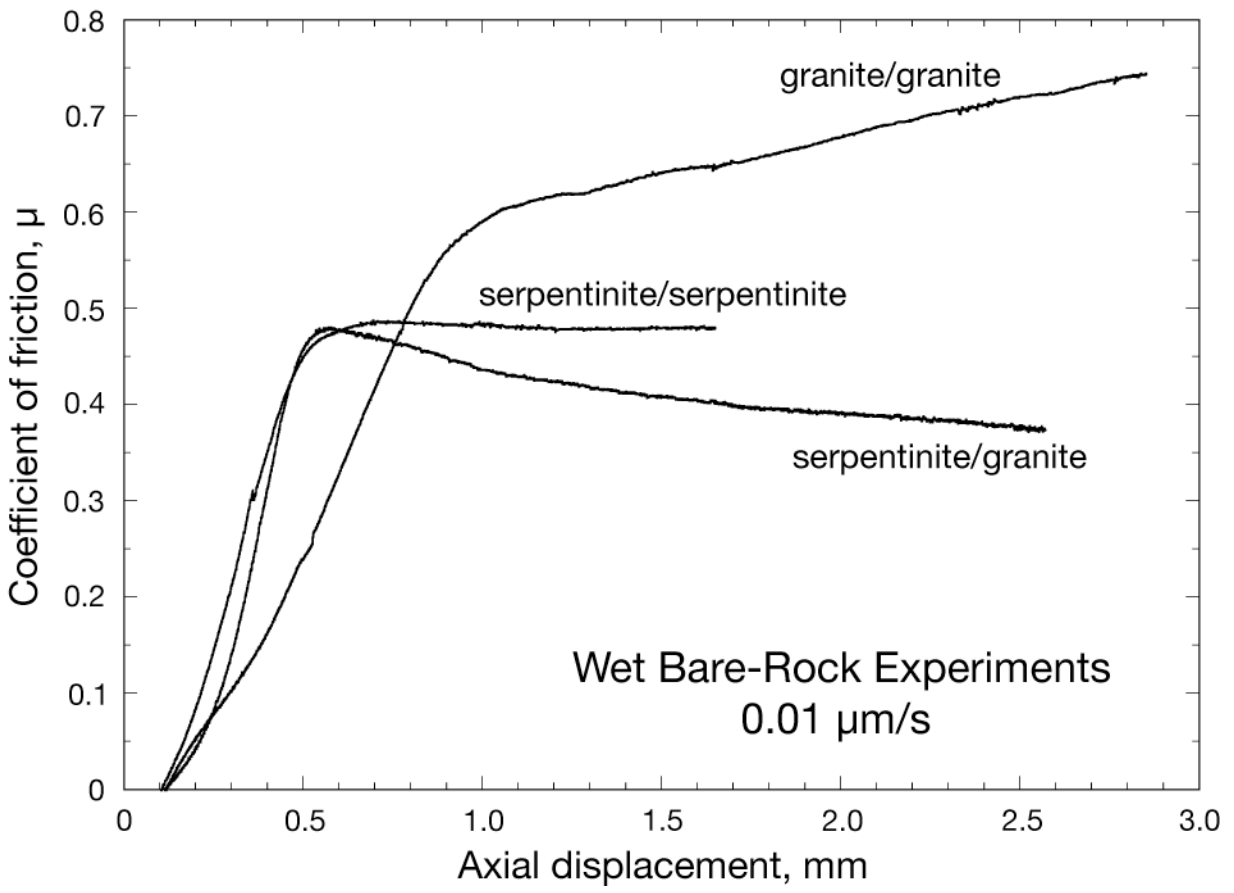


Figure 2

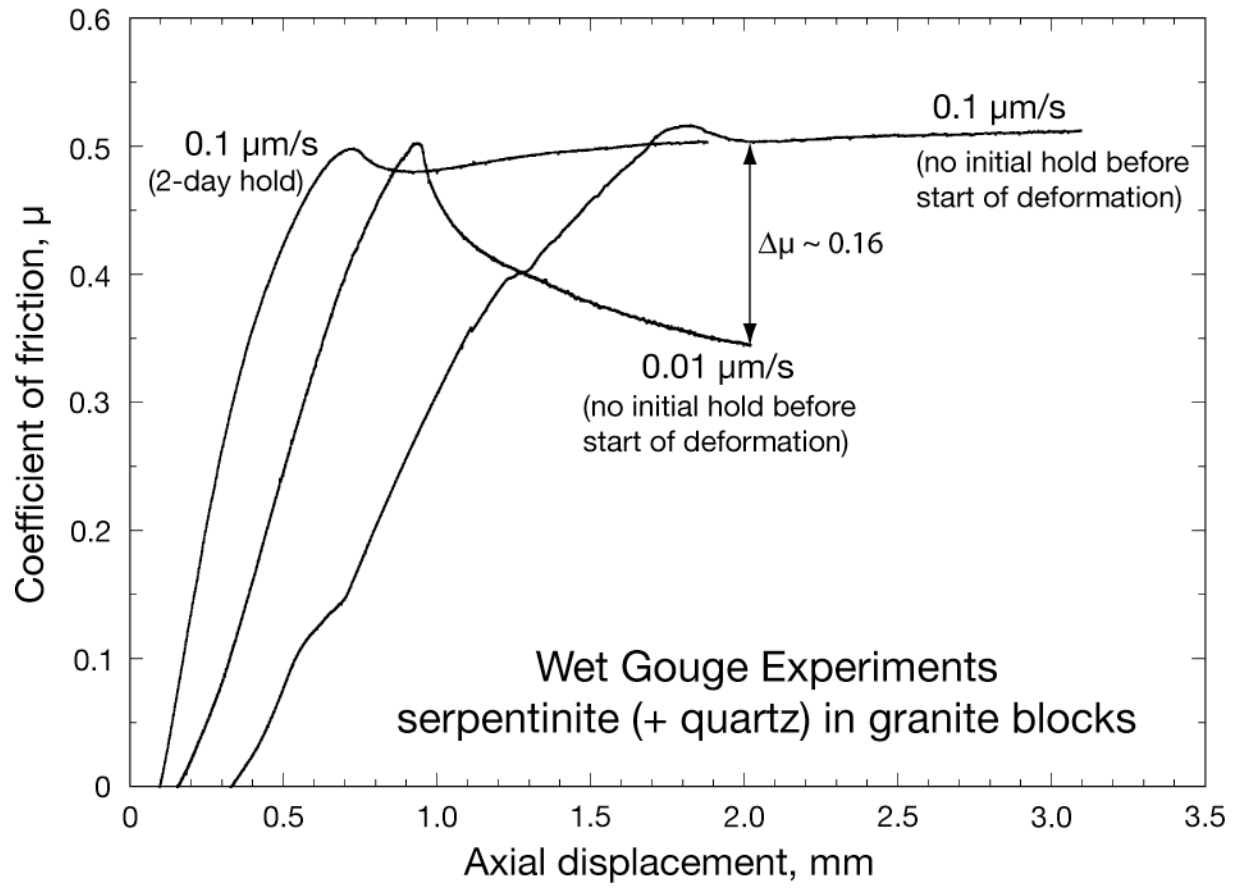


Figure 3

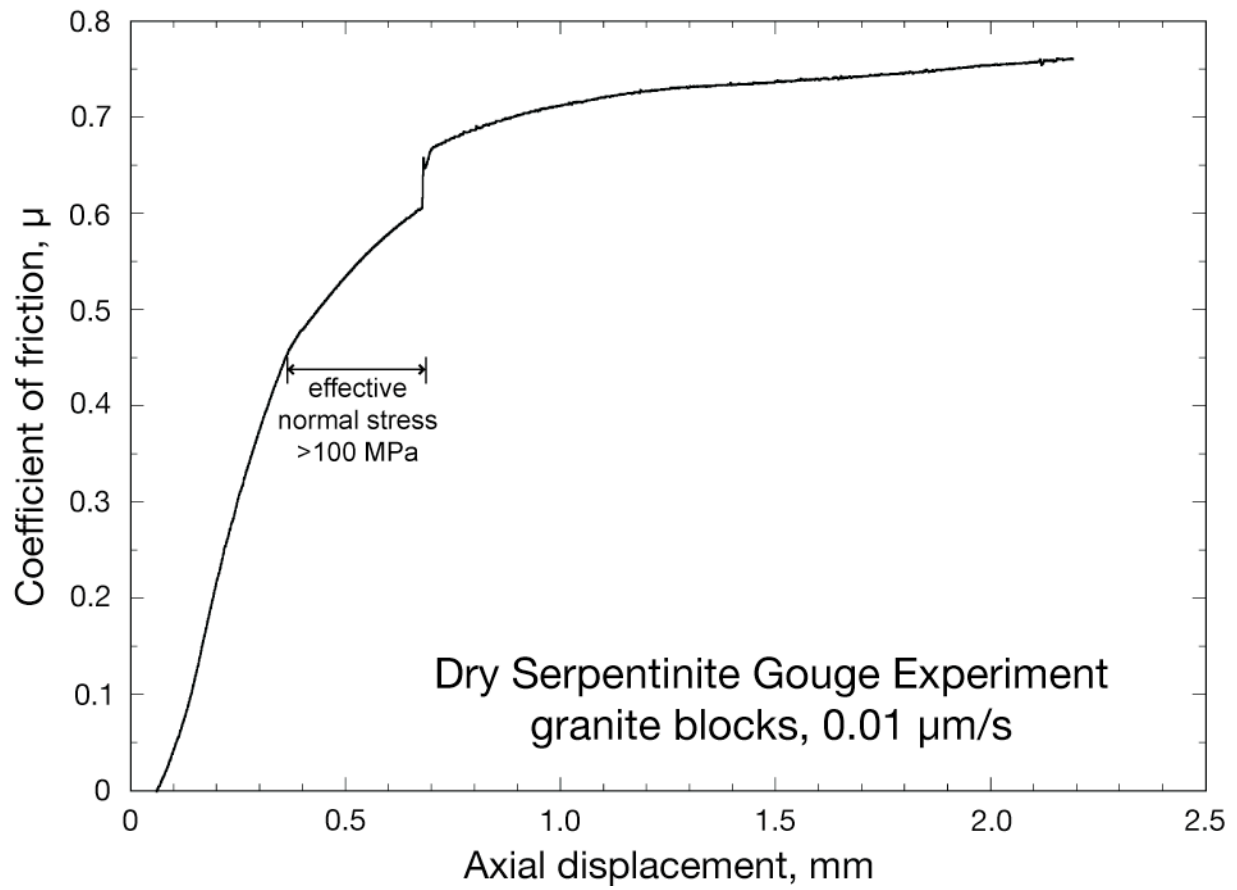


Figure 4

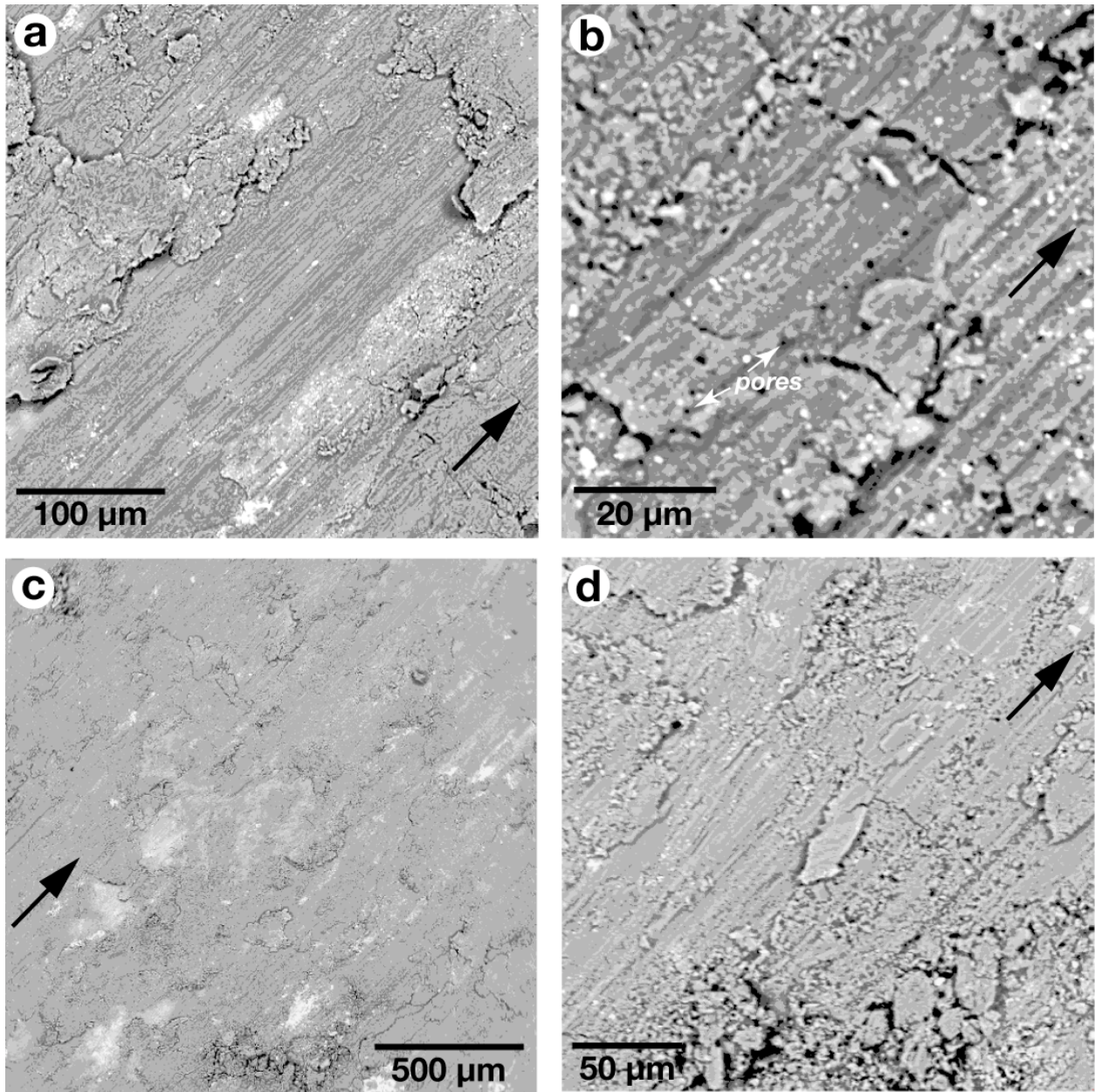


Figure 5

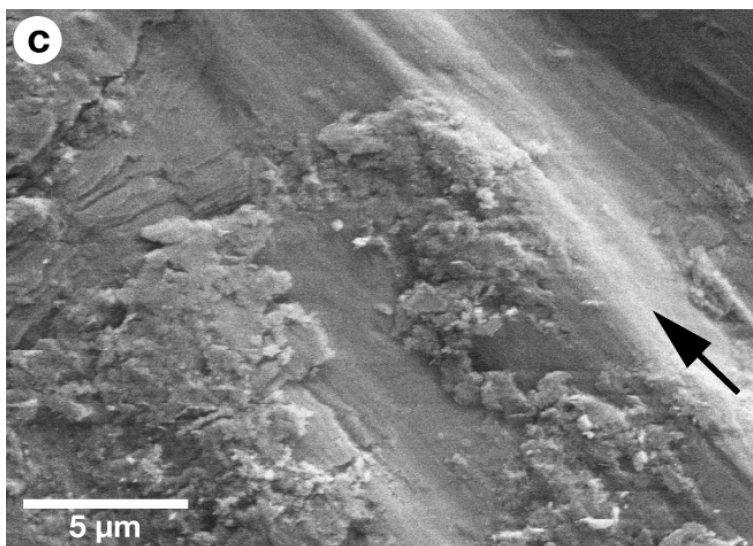
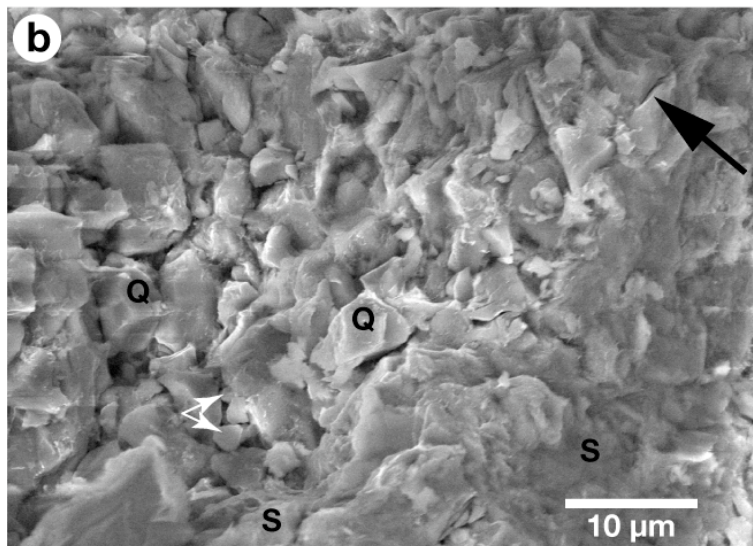
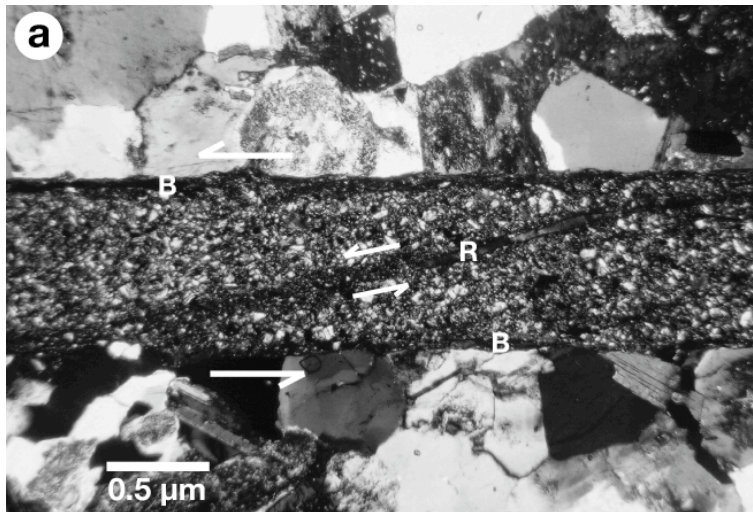


Figure 6

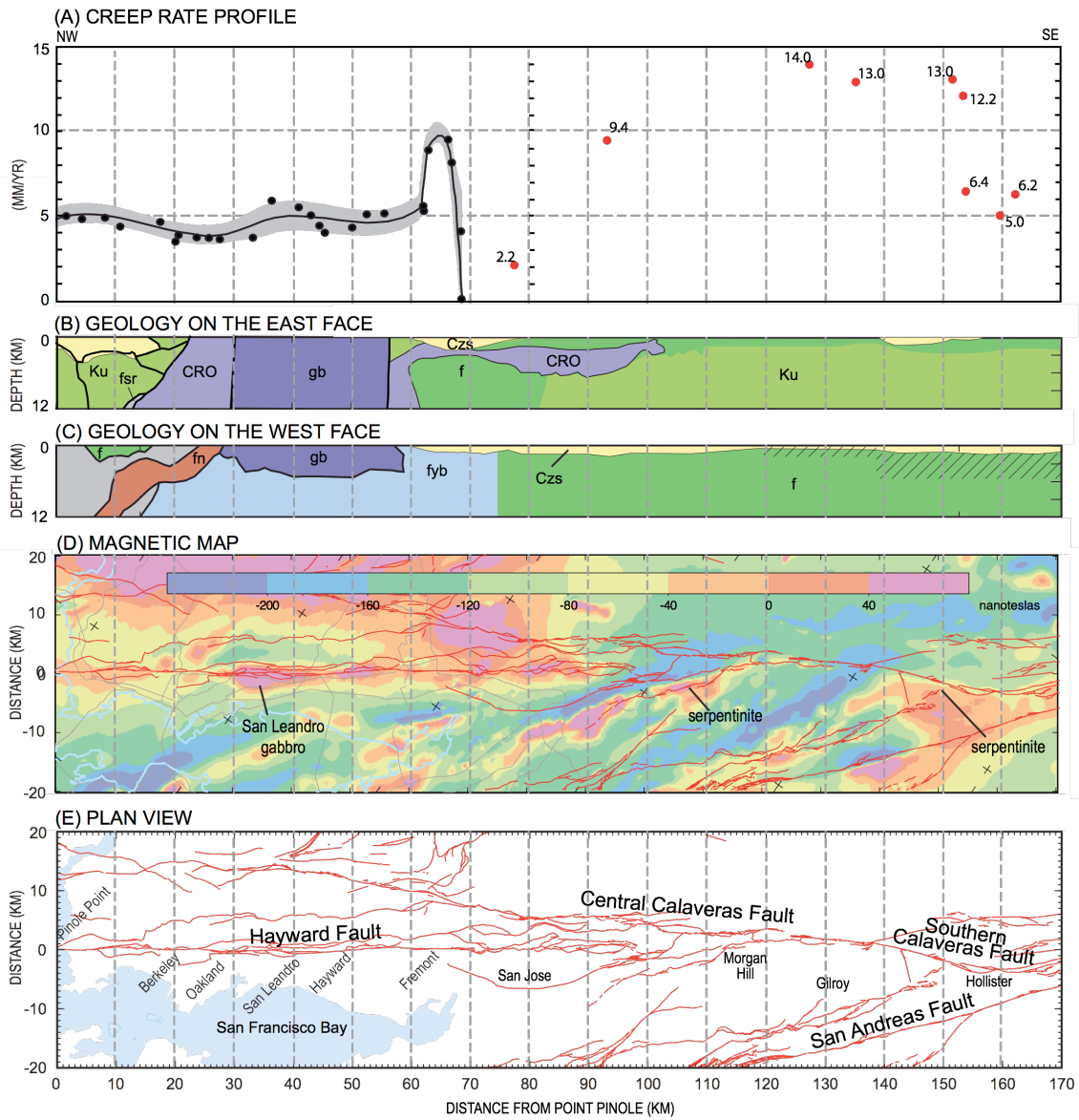


Figure 7